CrystEngComm

PAPER

View Article Online
View Journal | View Issue

Cite this: *CrystEngComm*, 2014, **16**, 5021

Vanadium-doped TiO_2 anatase nanostructures: the role of V in solid solution formation and its effect on the optical properties†

W. Avansi Jr.,*[a] R. Arenal,[bc] V. R. de Mendonça,[d] C. Ribeiro[e] and E. Longo[f]

Received 19th November 2013,
Accepted 3rd March 2014

DOI: 10.1039/c3ce42356e

www.rsc.org/crystengcomm

A facile and environmentally friendly synthesis approach for the production of vanadium doped titanium dioxide ($V_xTi_{1-x}O_2$) nanostructures was demonstrated *via* hydrothermal decomposition of vanadium and titanium peroxo-complexes. The effect of vanadium addition on the structural and morphological properties of $V_xTi_{1-x}O_2$ nanocrystals was investigated by X-ray diffraction (XRD) and electron microscopy techniques. XRD analysis showed that all $V_xTi_{1-x}O_2$ samples presented only the TiO_2 anatase crystalline phase and, despite the different amounts of vanadium ions, the single crystalline nature was preserved. Increasing V contents resulted in morphological evolution, from anisotropic to isotropic structures. X-ray absorption spectroscopy (XAS) and electron energy loss spectroscopy (EELS) have been employed for investigating the atomic composition and configuration of these nanostructures. XAS measurements at the K-edges (for V and Ti) revealed that V ions occupy the Ti^{4+}-site, which confirms the doping effect. Furthermore, high-angle annular dark-field (HAADF) imaging, combined with EELS mapping, indicated that the vanadium ions were homogeneously distributed in the structure without any kind of segregation. These morphological and compositional modifications upon vanadium addition led to evolution of the TiO_2 optical properties.

1. Introduction

Titanium dioxide (TiO_2) nanostructures, particularly in the anatase phase, have attracted significant attention because of their interesting physical and chemical properties.[1–5] As a matter of fact, these nanostructures have already been employed in several applications,[1–5] having a significant role in heterogeneous photocatalysis.[2,5] In this sense, the improvement of the photocatalytic activity of TiO_2 is one of the main aspects that should be addressed for the application of these nanostructures.[6–9] The TiO_2 has a band gap ~3.2 eV (UV spectral range), which corresponds to around 4% of the sun light, limiting its use in photocatalysis.[9–11] Thus, in order to overcome this limiting aspect and to improve the efficient use of solar energy, which is one of the main challenges in the heterogeneous photocatalysis field, a shift of the band gap of TiO_2 to the visible region is required. Extensive research has been made in order to modify the band gap of TiO_2 anatase nanostructures to absorb wavelengths longer than 387 nm (3.2 eV) by introducing metal or nonmetal dopants.[6,7,9,10,12–18] In this way, vanadium-doped TiO_2 can show suitable characteristics for its application as a photocatalyst and different synthesis methods have been proposed to achieve this goal.[7,14–16]

Technological applications of nanostructured materials are directly related to several factors such as the morphology, size, crystalline phase and activity of a specific crystalline plane.[3,19–23] Additionally, it is worth mentioning that the localization and the atomic configuration of the doped atoms in the pristine nanocrystalline structure have a strong influence on the final properties of any material.[14,24–30] Furthermore, the presence and distribution of the doping elements in the nanostructures can result in a different crystal growth mechanism, influencing the final shape of the nanoparticles.[24–26,31–33] In all of these cases, a controllable and simple synthesis process is required to achieve these goals. Recently, several studies have reported the synthesis of diverse nanostructures through the hydrothermal treatment of the peroxo-metal complex, which is considered a simple and environmentally friendly method to obtain nanostructures without contaminants like halide ions or organic compounds.[2,28,34–38] Concerning the particular case of this system (vanadium-doped TiO_2), the peroxo-complex method

[a] *Departamento de Física, Universidade Federal de São Carlos - UFSCar, P.O. Box 676, CEP, 13565-905 São Carlos, São Paulo, Brazil. E-mail: wavansi@pq.cnpq.br*
[b] *Laboratorio de Microscopias Avanzadas (LMA), Instituto de Nanociencia de Aragon (INA), Universidad de Zaragoza, Calle Mariano Esquillor, 50018 Zaragoza, Spain*
[c] *ARAID Fundation, Calle Mariano de Luna, 50018 Zaragoza, Spain*
[d] *Departamento de Química, Universidade Federal de São Carlos - UFSCar, São Carlos, Brazil*
[e] *Laboratório Nacional de Nanotecnologia aplicada ao Agronegócio - LNNA, Embrapa Instrumentação, 13560-970-São Carlos, SP, Brazil*
[f] *Instituto de Química, Universidade Estadual Paulista, Araraquara, São Paulo, Brazil*

† Electronic supplementary information (ESI) available. See DOI: 10.1039/c3ce42356e

is very appropriate because both Ti and V can be complexed by hydrogen peroxide, forming soluble solutions.[34,36] This is an optimum strategy for improving the homogeneity during the hydrothermal process, leading to an easy doping process.

In this work, we report a controlled, simple and environmentally friendly methodology to obtain vanadium doped TiO_2 ($V_xTi_{1-x}O_2$) nanostructures with different amounts of V ions as the doping element. We have also developed a systematic and detailed study of the fabricated nanostructures *via* macroscopic and local (atomic) analytical techniques. We show that vanadium (V) is uniformly incorporated in the TiO_2 structure and that this incorporation leads to modification of $V_xTi_{1-x}O_2$ nanostructures' optical properties (redshift of the band gap from UV to the visible light range). Additionally, morphological and structural evolution with increasing V content has also been monitored.

2. Experimental section

2.1. Synthesis

$V_xTi_{1-x}O_2$ samples were obtained through the simultaneous decomposition of peroxo metal complexes by hydrothermal treatment. A peroxo titanium complex was obtained according to the procedure described by Ribeiro *et al.*[37] In a typical synthesis process, a specific amount of metallic Ti (99.7%, Aldrich) was added in 80 mL of H_2O_2–NH_3 (both 29.0%, Synth) solution. This solution was left in an ice water bath until complete dissolution of the metal, resulting in a yellow transparent aqueous solution of the complex. Peroxo vanadium complexes were prepared by dissolving V_2O_5 powder (Puratronic, 99.9%) in H_2O_2 solution, as described by Avansi *et al.*[34] The strategy to obtain such doped materials is to employ conditions where one of them is not supposed to crystallize, remaining as an ion in solution during the nucleation and growth. In the next step, appropriate amounts of the complex solutions were mixed in order to obtain $V_xTi_{1-x}O_2$ samples with different V amounts, annealing the resultant mixture in a hydrothermal cell with a fine temperature control. The synthesis conditions were set at 200 °C for 4 hours for all of the samples. After the treatment, the produced samples were rapidly quenched in an ice bath and collected by centrifugation. Then, the as-obtained samples were washed several times with distilled water and isopropanol and finally, they were dried at 60 °C for 8 hours.

2.2. Characterization

In order to determine the amount of ions remaining in solution after the synthesis, the liquid phases obtained after centrifugation and the powder resulting from the separation were analyzed by an Inductively Coupled Plasma Atomic Emission Spectrometer (ICP-AES), Varian model VISTA-MPX, with radial configuration. The values obtained were used to estimate the real doping values, by subtracting these values from the amount added for the reaction, before the hydrothermal treatment. Standard calibration curves with 6 points were obtained by linear regression of intensities from a series of multi-element standards with variable mass concentrations for each analysis.

Crystalline phases present in the final products were investigated by X-ray diffraction (XRD) using a Shimadzu XRD 6000 diffractometer, with Cu Kα (λ = 1.5406 Å) radiation, an angular pass of 0.02° and an exposure time of 1 s. Crystallographic coherence lengths were determined according to Scherrer's equation, deconvoluting each peak using pseudo-Voigt approximation to determine the full width at half maximum (FWHM).[39]

The sizes and morphologies of the samples were determined by field emission scanning electron microscopy (FE-SEM) using a JEOL JSM6701F microscope. The as-obtained samples were also studied by transmission electron microscopy (TEM). Conventional TEM and high-resolution (HRTEM) studies were performed using a JEM 2100 URP (operating at 200 kV) and an aberration-corrected FEI Titan-Cube microscope operating at 80 kV equipped with a Cs corrector (CETCOR from CEOS GmbH). Atomic resolution electron energy loss spectroscopy (EELS) measurements as well as HR scanning TEM (HRSTEM) studies were performed using a probe-corrected STEM FEI Titan Low-Base 60–300 operating at 80 kV (fitted with a X-FEG® gun and a Cs-probe corrector (CESCOR from CEOS GmbH)). EEL spectra were recorded in the spectrum-imaging mode[40,41] using a Gatan GIF Tridiem ESR spectrometer. The convergent semi-angle was 25 mrad, the collection semi-angle was 80 mrad and the energy resolution was ~1.2 eV. Additionally, the chemical analyses of the samples were performed by Energy Dispersive X-ray Spectroscopy (EDS) using an EDS Thermo-Noran equipped with a Si detector attached to the JEOL JEM 2100.

The variation in the electronic and local atomic structure was investigated by X-ray Absorption Spectroscopy (XAS). XANES (X-ray absorption near edge structure) spectra were measured at the V and Ti K-edges using the D08B-XAFS2 beamline at the Brazilian Synchrotron Light Laboratory (LNLS). XANES spectra were collected in transmission mode at room temperature using a Si (111) channel-cut monochromator, measured from 40 eV below and 80 eV above the edge, with an energy step of 0.3 eV near the edge region. To provide good energy reproducibility during the collection of XANES data, the energy calibration of the monochromator was checked while the data were being collected, using a V or Ti metal foil. All of the data were normalized to the edge and aligned in energy. The XANES spectra were analyzed using the IFEFFIT package.[42,43]

In order to analyze the effect of V ions on the optical properties of TiO_2 materials, Diffuse reflectance UV–vis spectra (DRS) were acquired using a Cary 5G spectrophotometer in the 250–800 nm range. The as-obtained spectra were converted by the Kubelka–Munk function[44] and normalized. The band gap of the samples was calculated using the equation proposed by Tauc *et al.*[45]

3. Results and discussion

The quantitative chemical composition of the as-synthesized samples, determined by the ICP-AES technique, confirmed the presence of vanadium atoms in the TiO_2 nanostructures

and the chemical composition of the $V_xTi_{1-x}O_2$ samples, where x = 0.04, 0.07, 0.16, 0.25 and 0.40 (mol%). Thus, the chemical analyses confirmed doping amounts in the range of 4–40% of V (in molar ratio to Ti). Additionally, the EDS analysis performed on the $V_{0.40}Ti_{0.60}O_2$ samples confirmed the presence of only V and Ti elements, as shown in Fig. 1. It is worth mentioning that the small peak at around 1.0 keV visible in this spectrum corresponds to the presence of copper element from TEM grid.

Fig. 2 presents the X-ray diffraction patterns of the as-synthesized samples. It is worth noting that, despite the increasing amount of V, only the TiO_2 anatase phase was identified in all studied samples, even at the molar ratio of 0.40. As we have shown above, vanadium has been detected *via* different analytical techniques. Nevertheless, the fact that no vanadium phases (such as the V_2O_5 orthorhombic phase) have been observed in these XRD measurements indicates that the V atoms are incorporated in the TiO_2 crystalline structures. These results are supported by the recent studies of Le Roy *et al.* which reported the epitaxially grown anatase $(Ti_{1-x}V_x)O_2$ films with a solubility limit of around 21% of V atoms in anatase TiO_2.[46]

In order to investigate the effect of the V amount on crystallite sizes, specific crystallographic directions were calculated using the Scherrer equation,[39] as schematically shown in Fig. 3.

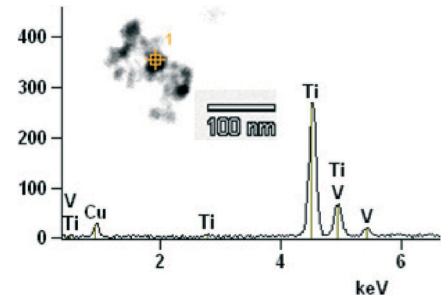

Fig. 1 The EDS spectrum recorded in the region marked in the bright-field STEM image in the inset. For illustration purposes, only the EDS results for the $V_{0.40}Ti_{0.60}O_2$ samples will be presented here.

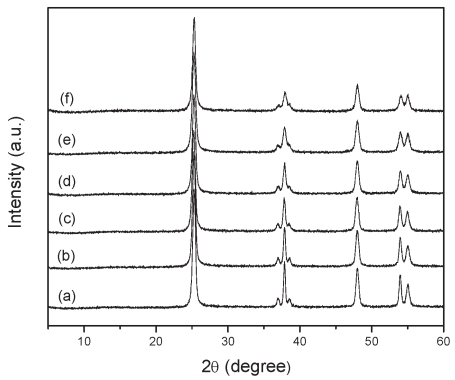

Fig. 2 XRD patterns of the as-synthesized samples: (a) TiO_2 (pristine); (b) $V_{0.04}Ti_{0.96}O_2$; (c) $V_{0.07}Ti_{0.93}O_2$; (d) $V_{0.16}Ti_{0.74}O_2$; (e) $V_{0.25}Ti_{0.75}O_2$ and (f) $V_{0.40}Ti_{0.60}O_2$. The observed reflections correspond to the TiO_2 anatase phase (JCPDS #21-1272).

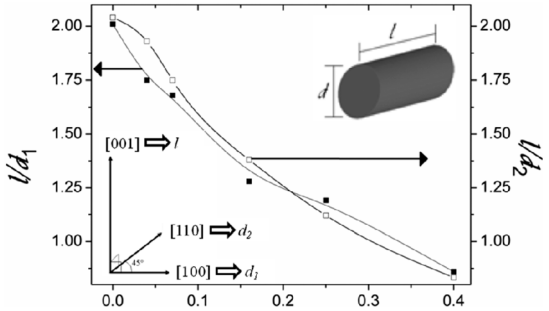

Fig. 3 Relation between V/Ti molar ratio and anisotropy in the as-synthesized samples.

This figure displays the plot of the ratio between the crystallite sizes on those planes and the V/Ti molar ratio in the different samples. The ratio between the values of the crystallite size in [004], parallel to [001], and [200] or [220], parallel to [100] and [110], respectively, can be understood as an indication of the materials' anisotropy, since [100] and [110] are in the same plane which is perpendicular to the [001] direction.[47] Preferential growth in the [001] direction can be explained by the fact that (001) planes are the most energetic facets in the TiO_2 anatase crystalline structure.[48,49] The results in Fig. 3 show that the crystallite size in the [001] direction of $V_{0.04}Ti_{0.96}O_2$ is twice the crystallite size in the perpendicular directions. In fact, the ratio between the values of the crystalline size, presented in Fig. 3, continually decreases with increasing V content. These results suggest the presence of anisotropic nanostructures in the samples with lower V amounts, leading then to evolution to isotropic structures with increasing V content.

Fig. 4 presents FE-SEM images of the as-obtained $V_xTi_{1-x}O_2$ samples. An analysis of the images depicted in Fig. 4a clearly shows that the morphology of the TiO_2 (pristine) samples is based on the nanorod shape. Moreover, an analysis of the results presented in Fig. 4b–f confirms that with the increase in the vanadium content, anisotropic nanostructures (for the samples with lower V amounts) lead to evolution to isotropic structures, as observed in Fig. 3. The mean size estimated by the SEM images related to length (l) for the $V_xTi_{1-x}O_2$ samples, where x = 0, 0.04, 0.07, 0.16, 0.25 and 0.40, was equal to (96.2 ± 29.0), (60.8 ± 14.1), (45.7 ± 11.7), (38.4 ± 6.6), (30.1 ± 4.9) and (32.6 ± 4.2) nm, respectively. (see Fig. S1 in the ESI†). These results show the decrease in the size of the nanostructure as a function of the V content up to x = 0.25.

The morphological evolution of these samples upon V addition has also been confirmed by TEM analysis (see Fig. 5). Fig. 5a shows the presence of nanorods (anisotropic structures) with a length of around 100 nm. In Fig. 5b–e, it is possible to observe a continuous decrease in the length of the nanorods and a slight difference in the diameter, which can be considered constant. For the higher V amount, sample $V_{0.40}Ti_{0.60}O_2$, Fig. 5f shows almost isotropic nanoparticles, in good agreement with XRD and SEM results.

Fig. 6 displays the HRTEM analyses of the most representative samples. HRTEM images and Fourier Transform (FT)

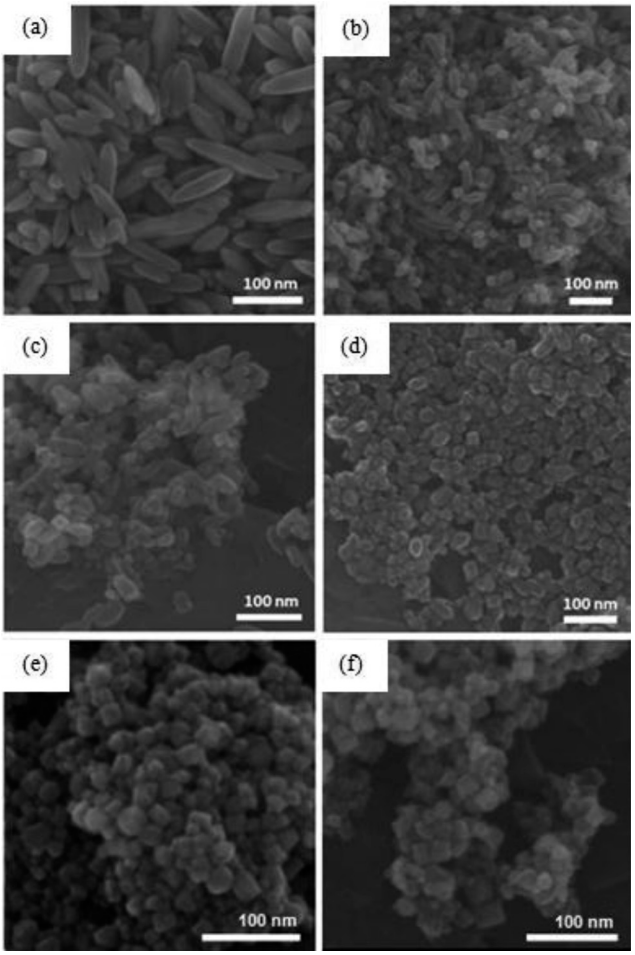

Fig. 4 SEM images of the as-synthesized samples: (a) TiO_2 (pristine); (b) $V_{0.04}Ti_{0.96}O_2$; (c) $V_{0.07}Ti_{0.93}O_2$; (d) $V_{0.16}Ti_{0.74}O_2$; (e) $V_{0.25}Ti_{0.75}O_2$ and (f) $V_{0.40}Ti_{0.60}O_2$.

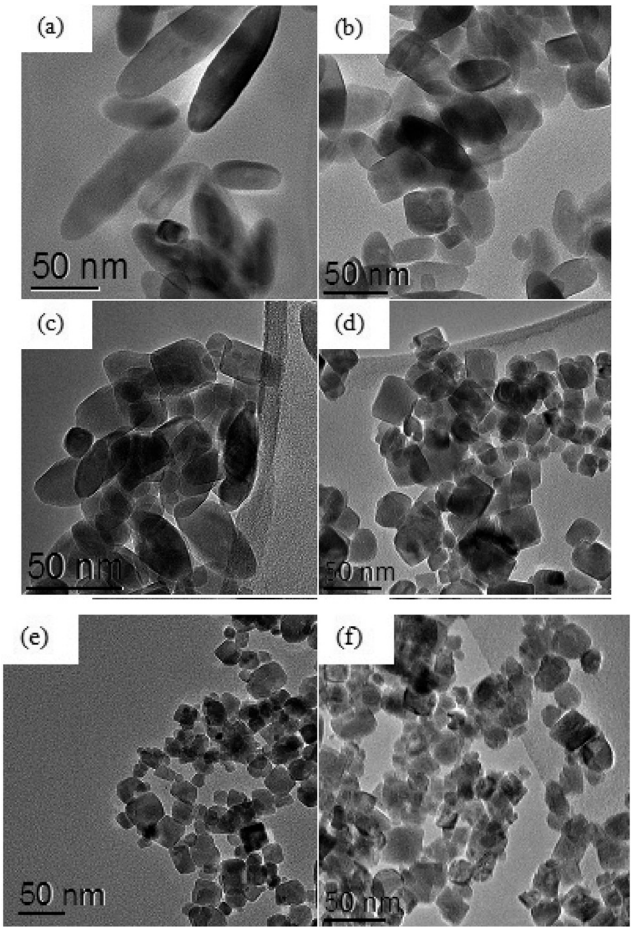

Fig. 5 TEM images of the as-synthesized samples: (a) TiO_2 (pristine); (b) $V_{0.04}Ti_{0.96}O_2$; (c) $V_{0.07}Ti_{0.93}O_2$; (d) $V_{0.16}Ti_{0.74}O_2$; (e) $V_{0.25}Ti_{0.75}O_2$ and (f) $V_{0.40}Ti_{0.60}O_2$.

of the regions displayed in Fig. 6 show that, despite the different amounts of V ions in the TiO_2 structure, the monocrystalline nature of the samples was preserved. Additionally, HRTEM and their respective FT results do not reveal any evidence of secondary crystallographic phases or even local aggregation of V atoms (or V-rich nanoclusters). This fact strongly suggests that V atoms are incorporated in the TiO_2 structure even for V content up to 40%, which again is in good agreement with XRD results. For pristine TiO_2 and $V_{0.04}Ti_{0.96}O_2$ samples, the HRTEM image and FT results (Fig. 6a) indicate that these nanorods grew along the [001] direction, as previously observed in the XRD data (see Fig. 2). Furthermore, it is worth mentioning that the isotropic nanostructures having the smallest sizes, which are the ones in which vanadium content was around 16 and 40%, present a preferential exposure of the (101) crystalline plane (see Fig. 4 and 6c, respectively).

The observed morphology changes can be described in terms of surface energy for different crystalline planes.[31,50,51] Some previous studies reported that the average surface energies of anatase TiO_2 crystals are 0.90 J m^{-2} for {001}, 0.53 J m^{-2}

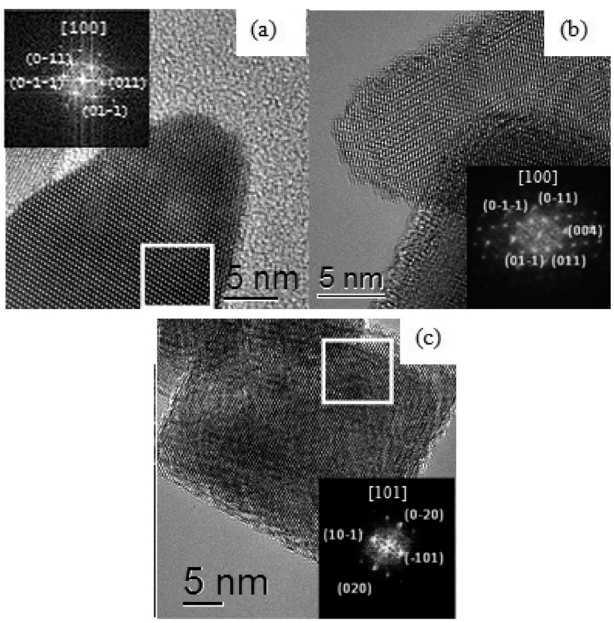

Fig. 6 HRTEM images of the samples and respective Fourier Transform (FT): (a) pristine; (b) $V_{0.04}Ti_{0.96}O_2$ and (c) $V_{0.40}Ti_{0.60}O_2$.

for {100} and 0.44 J m^{-2} for {101}.[48–50,52] These values indicate that anatase TiO_2 crystals are usually dominated by {101} facets, which are the most stable thermodynamically. The HRTEM results reveal that the presence of V ions in the TiO_2 crystals leads to a quick preferential exposure of (101) planes, without requiring a post-treatment (such as thermal annealing treatment). The presence and the distribution of doping elements have an important effect on the morphology and structure, which can induce a change in the surface energy and, consequently, in the crystal growth mechanism.[31,33] In fact, from the results reported here, V (as the dopant) plays a significant role in the crystal growth mechanism, which is very important to obtain doped nanostructures with altered shapes.

The atomic environment of these samples was also studied by XANES, focusing on the vanadium (V) and titanium (Ti) K edges. To enable comparison between V and Ti XANES spectra, the energy has been rescaled to the respective absorption K edges calculated from the first derivative of the spectra. No changes were observed in the spectra recorded on all synthesized samples, indicating that the V-state in the structure is the same for all cases. Thus, for the sake of clarity, only the result of $V_{0.40}Ti_{0.60}O_2$ samples is presented. Fig. 7 shows the normalized XANES spectra of the $V_{0.40}Ti_{0.60}O_2$ sample (V-K edge) and the reference compounds (V_2O_5 orthorhombic phase, VO_2 monoclinic phase and TiO_2 anatase phase). In order to evaluate the environment of V atoms in the TiO_2 lattice, XANES measurements on the Ti K-edge were carried out for the pristine TiO_2 anatase phase. The spectral features in Fig. 7 reflect the typical anatase structure of the TiO_2 lattice, with three major features in the pre-edge region.[2,36,53] Concerning the XANES spectra of the reference compounds based on V (V_2O_5 orthorhombic phase and VO_2 monoclinic phase), the analysis of the V-K edge shows an intense pre-edge peak, from the transition from V 1s states to V 3d states.[34,54–57] However, it is worth mentioning that in centrosymmetric systems, this transition is forbidden by the dipole selection rules, although it is allowed in noncentrosymmetric systems due to the hybridization between the V 3d and O 2p states.[34,54–57] The environment of V ions in the TiO_2 lattice was studied by comparison of the XANES spectra obtained at the Ti and V-K edges in the $V_{0.40}Ti_{0.60}O_2$ sample (Fig. 7). As can be seen, despite the expected differences in the pre-edge region, the XANES spectra of the V and Ti-K edges are similar, indicating that a substantial number of vanadium atoms are substitutionally occupying the anatase lattice.

High-resolution scanning transmission electron microscopy (HRSTEM) is a powerful characterization technique in materials science because it allows the possibility of combining high-resolution imaging and spectroscopy, even at the atomic level.[33,41,58–62] As we have already shown and mentioned, no significant changes have been observed concerning the atomic configuration of these $V_xTi_{1-x}O_2$ nanostructures. Therefore, we will only present the results concerning the $V_{0.40}Ti_{0.60}O_2$ sample. Fig. 8(a) displays a high-resolution HAADF (high-angle annular dark-field) STEM image of an individual

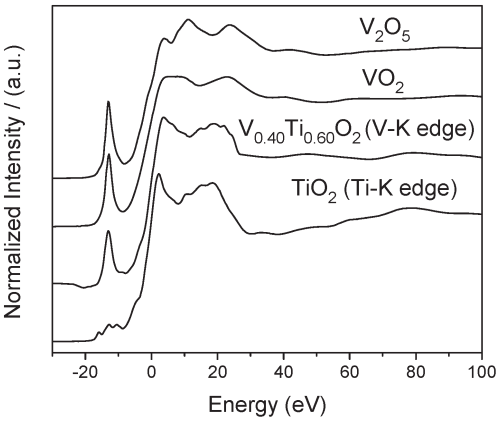

Fig. 7 Normalized XANES spectra at the vanadium (V) and titanium (Ti) K-edges. XANES spectra acquired for the sample $V_{0.40}Ti_{0.60}O_2$ and the reference compounds: V_2O_5 orthorhombic phase, VO_2 monoclinic phase and TiO_2 anatase phase. The XANES spectra were calibrated in energy using the point of inflection determined by the first derivative of the normalized XANES spectra.

nanocrystal of $V_{0.40}Ti_{0.60}O_2$. An EELS spectrum-line (SPLI)[40,41] has been recorded following the red line marked in Fig. 8(a). Among all of the spectra of this SPLI, ten consecutive spectra have been selected and added (see Fig. 8(b)). Characteristic signals corresponding to Ti–$L_{2,3}$, V–$L_{2,3}$, and O-K edges are visible in this EEL spectrum. This result confirms the chemical ICP and EDS analyses, showing the existence of these

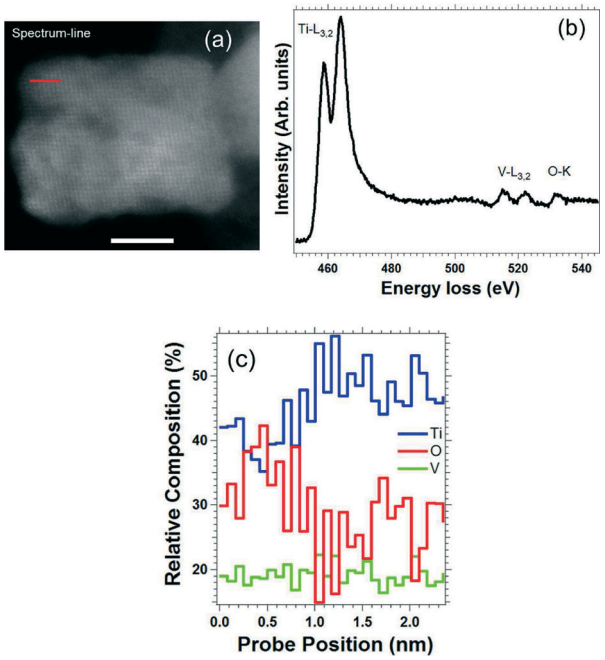

Fig. 8 (a) A high-resolution HAADF image of an individual nanocrystal of the $V_{0.40}Ti_{0.60}O_2$ sample. The scale bar is 5 nm. (b) The EEL spectrum sum of 10 EEL spectra extracted from the spectrum-line recorded in the red line marked in (a). (c) Relative composition (at.%) of titanium, vanadium and oxygen has been obtained after background subtraction and quantification analyses were carried out on the EEL spectrum in (b) on Ti–$L_{2,3}$, V–$L_{2,3}$ and O-K edges, respectively.

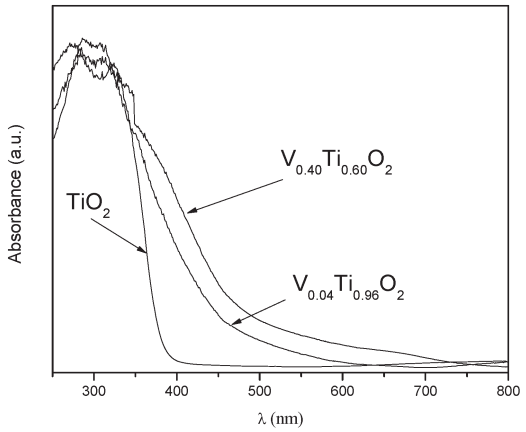

Fig. 9 Diffuse reflectance UV–vis spectra of TiO_2 and $V_xTi_{1-x}O_2$ samples (x = 0.04 and 0.40).

elements in the nanocrystals. The relative composition of each of these elements was obtained using standard quantification procedures[63] on the EELS spectra extracted from the SPLI (see Fig. 8c). From the profiles of the composition of these elements as a function of the probe position, we can observe that, as expected, the Ti and O contents are anti-correlated and that V is homogenously distributed in the nanostructure. Furthermore, it is worth mentioning that V distribution is similar to that of Ti ions. Thus, these results confirm preferential substitution of Ti by V ions without any kind of segregation between them, as observed by XANES spectroscopy.

In order to study the optical properties, the normalized reflectance data of selected samples was measured (Fig. 9). As expected, the incorporation of vanadium ions in the structure leads not only (and in parallel) to morphological and compositional changes but also to the modification of the band gap of these nanostructures. The pristine anatase TiO_2 has an absorption band edge at around 390 nm (see Fig. 9), which corresponds to a band gap in the UV at around 3.2 eV, in good agreement to previous studies.[6,7,9,10,13–18] For the $V_xTi_{1-x}O_2$ samples (x = 0.04 and 0.40) we can observe edge shifts to visible-light wavelengths. The estimated band gaps (following the x axis intercept) of the $V_xTi_{1-x}O_2$ samples (x = 0.04 and 0.40) were around 2.70 (460 nm) and 2.48 eV (500 nm). These results show that the incorporation of V results in edge shifts to longer wavelengths, *i.e.* in the visible-light wavelengths. These shifts could be attributed to transitions involving impurity levels, where the presence of V in the structure leads to a wider-band gap material.[6,7,9,10,13–18] In fact, according to Liu *et al.*, the presence of V^{4+} species in the structure causes the shift of absorption spectra to the visible light region.[7]

4. Conclusions

In summary, we have successfully synthesized $V_xTi_{1-x}O_2$ nanostructures using a simple and environmentally friendly hydrothermal method at low temperature and a short synthesis time. A morphological evolution from anisotropic to isotropic nanostructures has been observed as a function of V content. XANES and atomic-resolved EELS measurements revealed that vanadium ions occupy preferentially Ti^{4+}-sites. These morphological and compositional modifications lead to a redshift of the band gap of TiO_2 nanocrystals which can improve their technological applications. These results show that V as the dopant plays an important role in the crystal growth of the as-obtained nanostructures, which is critical to obtain doped nanostructures with altered shapes. On the other hand, we expect that the simple and efficient synthesis route proposed herein can be extended to the synthesis of different metal/nonmetal doped titanates nanostructures.

Acknowledgements

The authors gratefully acknowledge financial support from the Brazilian research funding agencies FAPESP and CNPq. We are also grateful to M. I. B. Bernardi for ICP-AES measurements. XANES measurements were performed in the National Laboratory of Synchrotron Light (LNLS), Campinas, Brasil. Some of the transmission electron microscopy images were recorded at the LME/LNNano/CNPEM. The rest of the microscopy measurements concerning HRTEM and HRSTEM-EELS were conducted in the Laboratorio de Microscopias Avanzadas at the Instituto de Nanociencia de Aragon – Universidad de Zaragoza (Spain). R.A. also acknowledges funding from grants 165-119 and 165-120 from U. de Zaragoza and from the ARAID foundation. Part of the research leading to these results has received funding from the European Union Seventh Framework Program under grant agreement 312483 - ESTEEM2 (Integrated Infrastructure Initiative – I3).

Notes and references

1 Y. Kwon, H. Kim, S. Lee, I.-J. Chin, T.-Y. Seong, W. I. Lee and C. Lee, *Sens. Actuators, B*, 2012, **173**, 441–446.
2 V. R. de Mendonca and C. Ribeiro, *Appl. Catal., B*, 2011, **105**, 298–305.
3 M. R. Hoffmann, S. T. Martin, W. Y. Choi and D. W. Bahnemann, *Chem. Rev.*, 1995, **95**, 69–96.
4 X. Chen and S. S. Mao, *Chem. Rev.*, 2007, **107**, 2891–2959.
5 M. D. Hernandez-Alonso, F. Fresno, S. Suarez and J. M. Coronado, *Energy Environ. Sci.*, 2009, **2**, 1231–1257.
6 S. George, S. Pokhrel, Z. Ji, B. L. Henderson, T. Xia, L. Li, J. I. Zink, A. E. Nel and L. Maedler, *J. Am. Chem. Soc.*, 2011, **133**, 11270–11278.
7 J. Liu, R. Han, Y. Zhao, H. Wang, W. Lu, T. Yu and Y. Zhang, *J. Phys. Chem. C*, 2011, **115**, 4507–4515.
8 C. H. Wang, C. L. Shao, X. T. Zhang and Y. C. Liu, *Inorg. Chem.*, 2009, **48**, 7261–7268.
9 W. Zhu, X. Qiu, V. Iancu, X.-Q. Chen, H. Pan, W. Wang, N. M. Dimitrijevic, T. Rajh, H. M. Meyer, III, M. P. Paranthaman, G. M. Stocks, H. H. Weitering, B. Gu, G. Eres and Z. Zhang, *Phys. Rev. Lett.*, 2009, **103**, 226401–226401.

10 X. Hong, Z. Luo and J. D. Batteas, *J. Solid State Chem.*, 2011, **184**, 2244–2249.
11 Y. Zhou, K. Vuille, A. Heel, B. Probst, R. Kontic and G. R. Patzke, *Appl. Catal., A*, 2010, **375**, 140–148.
12 Z. M. Wang, E. Sahle-Demessie and A. A. Hassan, *J. Nanotechnol.*, 2011, **11**, 209150.
13 G. B. Soares, B. Bravin, C. M. P. Vaz and C. Ribeiro, *Appl. Catal., B*, 2011, **106**, 287–294.
14 S.-M. Chang and W.-S. Liu, *Appl. Catal., B*, 2011, **101**, 333–342.
15 K. Chen, J. Li, W. Wang, Y. Zhang, X. Wang and H. Su, *Appl. Surf. Sci.*, 2011, **257**, 7276–7285.
16 S. Liu, T. Xie, Z. Chen and J. Wu, *Appl. Surf. Sci.*, 2009, **255**, 8587–8592.
17 C. Yogi, K. Kojima, T. Hashishin, N. Wada, Y. Inada, E. Della Gaspera, M. Bersani, A. Martucci, L. Liu and T.-K. Sham, *J. Phys. Chem. C*, 2011, **115**, 6554–6560.
18 F. Fresno, D. Tudela, J. M. Coronado, M. Fernandez-Garcia, A. B. Hungria and J. Soria, *Phys. Chem. Chem. Phys.*, 2006, **8**, 2421–2430.
19 U. I. Gaya and A. H. Abdullah, *J. Photochem. Photobiol., C*, 2008, **9**, 1–12.
20 C. Guillard, J. Disdier, J. M. Herrmann, C. Lehaut, T. Chopin, S. Malato and J. Blanco, *Catal. Today*, 1999, **54**, 217–228.
21 H. Mourao, V. R. de Mendonca, A. R. Malagutti and C. Ribeiro, *Quim. Nova*, 2009, **32**, 2181–2190.
22 F. Q. Dong, Q. S. Wu, J. Ma and Y. J. Chen, *Phys. Status Solidi A*, 2009, **206**, 59–63.
23 T. R. Giraldi, G. V. F. Santos, V. R. Mendonça, C. Ribeiro and I. T. Weber, *J. Nanosci. Nanotechnol.*, 2011, **11**, 1–6.
24 N. Han, L. Y. Chai, Q. Wang, Y. J. Tian, P. Y. Deng and Y. F. Chen, *Sens. Actuators, B*, **147**, 525–530.
25 T. M. Milao, J. F. A. Oliveira, V. D. Araujo and M. I. B. Bernardi, *J. Therm. Anal. Calorim.*, 2011, **103**, 873–877.
26 Y. F. Yang, Y. Z. Jin, H. P. He, Q. L. Wang, Y. Tu, H. M. Lu and Z. Z. Ye, *J. Am. Chem. Soc.*, 2010, **132**, 13381–13394.
27 R. S. Devan, R. A. Patil, J.-H. Lin and Y.-R. Ma, *Adv. Funct. Mater.*, 2012, **22**, 3326–3370.
28 J.-Y. Piquemal, E. Briot and J.-M. Bregeault, *Dalton Trans.*, 2013, **42**, 29–45.
29 P. Ayala, R. Arenal, A. Loiseau, A. Rubio and T. Pichler, *Rev. Mod. Phys.*, 2010, **82**, 1843–1885.
30 P. Ayala, R. Arenal, M. Rummeli, A. Rubio and T. Pichler, *Carbon*, 2011, **48**, 575–586.
31 M. Alfredsson, F. Cora, D. P. Dobson, J. Davy, J. P. Brodholt, S. C. Parker and G. D. Price, *Surf. Sci.*, 2007, **601**, 4793–4800.
32 L. F. da Silva, W. Avansi Jr., M. L. Moreira, J. Andres, E. Longo and V. R. Mastelaro, *CrystEngComm*, 2012, **14**, 4068–4073.
33 D. G. Stroppa, L. F. Zagonel, L. A. Montoro, E. R. Leite and A. J. Ramirez, *ChemPhysChem*, 2012, **13**, 1–8.
34 W. Avansi, C. Ribeiro, E. R. Leite and V. R. Mastelaro, *Cryst. Growth Des.*, 2009, **9**, 3626–3631.
35 W. Avansi, C. Ribeiro, E. R. Leite and V. R. Mastelaro, *Mater. Chem. Phys.*, 2011, **127**, 56–61.
36 C. Ribeiro, C. Vila, D. B. Stroppa, V. R. Mastelaro, J. Bettini, E. Longo and E. R. Leite, *J. Phys. Chem. C*, 2007, **111**, 5871–5875.
37 C. Ribeiro, C. M. Barrado, E. R. Camargo, E. Longo and E. R. Leite, *Chem.–Eur. J.*, 2009, **15**, 2217–2222.
38 Y. Wang and G. Cao, *Chem. Mater.*, 2006, **18**, 2787–2804.
39 *Elements of X-ray Diffraction*, ed. B. D. Cullity, Addison-Wesley Publish Company, 1967.
40 C. Jeanguillaume and C. Colliex, *Ultramicroscopy*, 1989, **28**, 252–257.
41 R. Arenal, F. de la Pena, O. Stephan, M. Walls, M. Tence, A. Loiseau and C. Colliex, *Ultramicroscopy*, 2008, **109**, 32–38.
42 M. Newville, *J. Synchrotron Radiat.*, 2001, **8**, 322–324.
43 M. Newville, *J. Synchrotron Radiat.*, 2001, **8**, 96–100.
44 K. Suzuki and K. Kijima, *Jpn. J. Appl. Phys., Part 1*, 2005, **44**, 2081–2082.
45 D. L. Wood and J. Tauc, *Phys. Rev. B: Condens. Matter Mater. Phys.*, 1972, **5**, 3144.
46 D. Le Roy, S. Valloppilly, R. Skomski, S. H. Liou and D. J. Sellmyer, *J. Appl. Phys.*, 2012, 111.
47 U. Diebold, *Surf. Sci. Rep.*, 2003, **48**, 53–229.
48 M. Lazzeri, A. Vittadini and A. Selloni, *Phys. Rev. B: Condens. Matter Mater. Phys.*, 2001, 63.
49 M. Lazzeri, A. Vittadini and A. Selloni, *Phys. Rev. B: Condens. Matter Mater. Phys.*, 2002, 65.
50 Y. Dai, C. M. Cobley, J. Zeng, Y. Sun and Y. Xia, *Nano Lett.*, 2009, **9**, 2455–2459.
51 R. L. Penn and J. F. Banfield, *Geochim. Cosmochim. Acta*, 1999, **63**, 1549–1557.
52 X. Han, Q. Kuang, M. Jin, Z. Xie and L. Zheng, *J. Am. Chem. Soc.*, 2009, **131**, 3152–3153.
53 F. Farges, *J. Non-Cryst. Solids*, 1996, **204**, 53–64.
54 A. N. Mansour, S. Dallek, P. H. Smith and W. M. Baker, *J. Electrochem. Soc.*, 2002, **149**, A1589–A1597.
55 S. Stizza, G. Mancini, M. Benfatto, C. R. Natoli, J. Garcia and A. Bianconi, *Phys. Rev. B: Condens. Matter Mater. Phys.*, 1989, **40**, 12229–12236.
56 W. Avansi, L. J. Q. Maia, C. Ribeiro, E. R. Leite and V. R. Mastelaro, *J. Nanopart. Res.*, 2011, **13**, 4937–4946.
57 F. Huguenin, E. A. Ticianelli and R. M. Torresi, *Electrochim. Acta*, 2002, **47**, 3179–3186.
58 C. Mitterbauer, G. Kothleitner, W. Grogger, H. Zandbergen, B. Freitag, P. Tiemeijer and F. Hofer, *Ultramicroscopy*, 2003, **96**, 469–480.
59 D. G. Stroppa, L. A. Montoro, A. Beltran, T. G. Conti, R. O. da Silva, J. Andres, E. Longo, E. R. Leite and A. J. Ramirez, *J. Am. Chem. Soc.*, 2009, **131**, 14544–14548.
60 S. Trasobares, M. Lopez-Haro, M. Kociak, K. March, F. de La Pena, J. A. Perez-Omil, J. J. Calvino, N. R. Lugg, A. J. D'Alfonso, L. J. Allen and C. Colliex, *Angew. Chem., Int. Ed.*, 2011, **50**, 868–872.
61 R. Arenal, X. Blase and A. Loiseau, *Adv. Phys.*, 2010, **59**, 101–179.
62 R. Arenal, O. Stephan, J. L. Cochon and A. Loiseau, *J. Am. Chem. Soc.*, 2007, **129**, 16183–16189.
63 R. Egerton, *Electron Energy-Loss Spectroscopy in the Electron Microscope*, Springer, 2011.